



1 **Abstract**

2 Marine atmosphere is usually considered to be a clean environment, while this study indicates
3 that the near-coast waters of South China Sea (SCS) suffered from even worse air quality
4 than coastal cities. The analyses were based on concurrent field measurements of target air
5 pollutants and meteorological parameters conducted at a suburban site (TC) and a nearby
6 marine site (WS) from August to November 2013. The observations showed that the levels of
7 primary air pollutants were significantly lower at WS than those at TC, while ozone (O₃)
8 value was greater at WS. Higher O₃ levels at WS were attributed to the weaker NO titration
9 and higher O₃ production rate because of stronger oxidative capacity of the atmosphere.
10 However, O₃ episodes were concurrently observed at both sites under certain meteorological
11 conditions, such as tropical cyclones, continental anticyclones and sea-land breezes (SLBs).
12 Driven by these synoptic systems and mesoscale recirculations, the interaction between
13 continental and marine air masses had profoundly changed the atmospheric composition and
14 subsequently influenced the formation and redistribution of O₃ in the coastal areas. When
15 continental air intruded into marine atmosphere, the O₃ pollution was magnified over SCS,
16 and the elevated O₃ (>100 ppbv) could overspread the sea boundary layer ~8 times the area of
17 Hong Kong. In some cases, the exaggerated O₃ pollution over the SCS was re-circulated to
18 the coastal inshore by sea breeze, leading to even aggravating O₃ pollution in coastal cities.
19 The findings are applicable to similar mesoscale environments around the world where the
20 maritime atmosphere is potentially influenced by severe continental air pollution.

21 **Key words:** Continental air pollution; Maritime atmosphere; Mesoscale recirculation; Ozone
22 photochemistry

23

24



1 **1 Introduction**

2 Ozone (O₃) plays a central role in photochemical oxidation processes in the troposphere via
3 direct reaction, photolysis and the subsequent reactions to produce the hydroxyl radical
4 (Monks et al., 2015; Seinfeld and Pandis, 2016). As a strong oxidant, O₃ at surface level is
5 recognized to be a threat to human health (WHO, 2003; Bell et al., 2007) and has a
6 detrimental impact on vegetation (Fowler et al., 2009) and built infrastructure (Kumar and
7 Imam, 2013). Tropospheric O₃ is also the third most important greenhouse gas (IPCC, 2014)
8 and is referred to a short-lived climate pollutant (Shindell et al., 2012).

9 To mitigate O₃ pollution in the troposphere, tremendous efforts from both scientific and
10 regulatory communities have been made since three decades ago (NRC, 1991; NARSTO,
11 2000; Monks et al., 2015). The O₃ levels started to decrease at many locations, such as
12 Jungfrauoch in Switzerland, Zugspitze in Germany, Mace Head in Ireland, as well as parts of
13 California and eastern US (Lefohn et al., 2010; Cui et al., 2011; Parrish et al., 2012; Lin et al.,
14 2017). However, increasing studies showed that surface O₃ was elevated rapidly in East Asia
15 in the last decade (Ding et al., 2008; Xu et al., 2008; Parrish et al., 2012; Zhang et al., 2014;
16 Lin et al., 2017; Wang et al., 2017a). For example, the observational data revealed that
17 regional O₃ concentrations increased at a rate of 0.86 ppbv yr⁻¹ in Pearl River Delta (PRD)
18 from 2006 to 2011 (Li et al., 2014), and at a rate of 0.56 ppbv yr⁻¹ in Hong Kong from 2005
19 to 2014 (Wang et al., 2017a).

20 Hong Kong and the adjacent PRD is the most industrialized region along the coast of South
21 China Sea (SCS), and is suffering from serious O₃ pollution (Zheng et al., 2010; Derwent et
22 al., 2013; Ling et al., 2013). Numerous studies demonstrated that in addition to long-range
23 transport (Chan, 2002; Guo et al., 2009; Wang et al., 2009) and local photochemical
24 production (Ding et al., 2013a), tropical cyclones and mesoscale circulations are conducive to
25 the occurrence of high O₃ events (Yin, 2004; Huang et al., 2005; Yang et al., 2012; Jiang et
26 al., 2015; Wei et al., 2016). In a number of studies, tropical cyclone has been considered as
27 the most conducive driver to the occurrence of O₃ episodes in Hong Kong (Yin, 2004; Ling et
28 al., 2013) for it generally causes peripheral subsidence, stagnation air and inversion layer,
29 which favor the production and accumulation of O₃.

30 Mesoscale circulations (*e.g.*, sea-land breezes (SLB) and mountain–valley breezes) also play
31 important roles in O₃ distribution and transport in the coastal cities like Hong Kong with



1 complex topography and land cover (Liu and Chan, 2002; Ding et al., 2004; Lu et al., 2009a;
2 Guo et al., 2013). For instance, Guo et al. (2013) demonstrated that upslope winds brought
3 pollutants including O₃ from low-lying areas to the peak of Mt Tai Mo Shan (957 m a.s.l.) in
4 Hong Kong. Ding et al. (2004) simulated a multi-day SLB related O₃ episode and discussed
5 the influence of SLB circulation on the transport of oxidant precursors, the residence time
6 and re-entry of photochemical compounds. Lu et al. (2010) simulated the SLB in the
7 2003/2004 winter and revealed that the urbanization of Shenzhen might significantly enhance
8 the sea breeze to the west of Hong Kong in the early afternoon, which worsened the local air
9 pollution.

10 Both coastal human activities and marine atmospheric cyclic behavior can significantly affect
11 the air pollution level in coastal urban environments (Adame et al., 2010; Velchev et al.,
12 2011). Exploring SLBs provides an important way to understand the interaction between
13 continental air and marine atmosphere which has long been a focus of coastal air quality,
14 global tropospheric chemistry and climate change research. Surprisingly, few studies
15 investigated SLBs in Hong Kong though about 70 SLB days per year on average were
16 observed in Hong Kong and the PRD region (Zhang and Zhang, 1997). Therefore, the
17 association between mesoscale recirculation and air pollutants over the SCS and subtropical
18 continental region is still not well established, which seriously limits our understanding on
19 the interplay of continental and marine air masses in this region. Furthermore, previous O₃
20 studies carried out in this region neither paid enough attention to the variations of volatile
21 organic compounds (VOCs, one important group of O₃ precursors) nor established any field
22 measurements on an island, an ideal site for observation of marine air mass with less
23 interference from local emissions, for understanding the O₃ pollution around the coastal
24 region of the SCS (Parrish et al., 1998). So far, only a handful of studies deeply evaluated the
25 chemical characteristics of air masses under various synoptic systems (Wang et al., 2005;
26 Guo et al., 2009, 2013).

27 This study aimed to comprehensively characterize interaction between continental
28 anthropogenic emissions and marine atmosphere over a coastal region of the SCS by
29 concurrent measurements and in-depth analysis of air pollutants at a marine site over SCS
30 and a suburban site in Hong Kong. Firstly, the spatial and temporal variations of
31 measurements were described to give an overall picture of the campaign, as well as to
32 directly evaluate how continental outflows polluted the marine atmosphere over the SCS.



1 After that, the chemical and meteorological characteristics of air masses associated with high
2 O₃ concentrations were explored. Finally, the interplay between the maritime and continental
3 air masses and its influence on regional air quality were discussed.

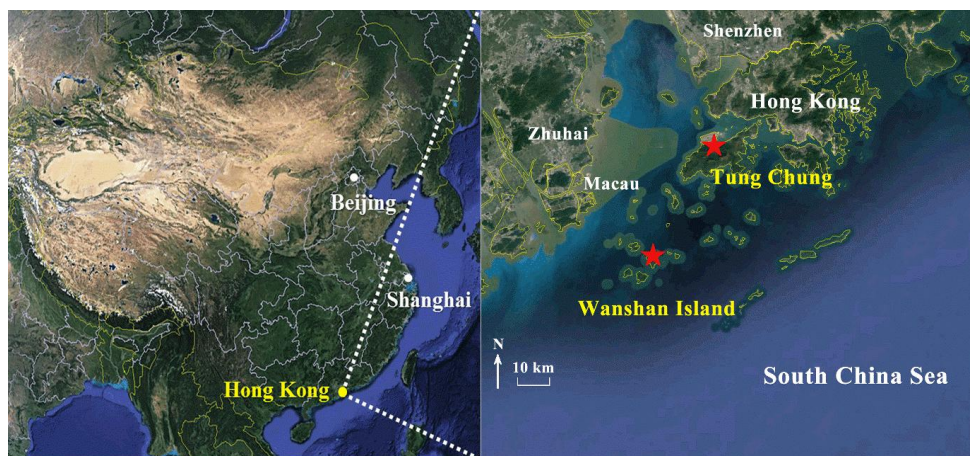
4 **2 Methodology**

5 **2.1 Sampling sites**

6 Field measurements were carried out concurrently at a suburban site and a marine site over
7 SCS (Figure 1). The suburban Tung Chung (TC, 22.29 °N, 113.94 °E) site, part of the Hong
8 Kong Environmental Protection Department (HKEPD) air quality monitoring network, is
9 located in southwestern Hong Kong, about 3 km south of the Hong Kong International
10 Airport at Chek Lap Kok with Hong Kong urban center about 20 km to the southwest and
11 Macau 38 km to the northeast. It is a newly-developed residential town adjacent to the busy
12 highway and railway lines. The sampling instruments were installed on the rooftop of a
13 building with a height of 27.5 m a.s.l. More detailed description of the TC site can be found
14 in our previous publications (Cheng et al., 2010a; Jiang et al., 2010).

15 The marine site, Wan Shan island (WS, 21.93 °N, 113.73 °E), is located 40 km southeast of
16 Zhuhai, and is bounded to the north by the Pearl River Estuary, with a straight distance of
17 about 44 km to TC. WS has an area of 8.1 km² and a population of about 3,000 with sparse
18 anthropogenic emissions at the island. The isolated island features a sub-tropical maritime
19 climate. The measurement site was set up on the rooftop of the National Marine
20 Environmental Monitoring Station with a height of about 65 m a.s.l.

21 High O₃ mixing ratios are frequently observed in Hong Kong in late summer and autumn
22 (Ling et al., 2013) when the northeast monsoon prevails. During this period, WS is right in
23 the downwind direction of TC, which facilitates the study of the interaction between the
24 inland pollution and the marine environment.



1

2 **Figure 1.** Locations of the sampling sites (red stars) and the surrounding environment.

3

4 **2.2 Measurement techniques**

5 *2.2.1 Measurements of trace gases and meteorological parameters*

6 The sampling campaign was conducted from 10 Aug. to 21 Nov. across late summer and
7 autumn in 2013. At WS, trace gases (*i.e.*, NO_x, O₃, SO₂ and CO) were continuously monitored
8 with a time resolution of 1 minute. NO-NO₂-NO_x was measured using a
9 chemiluminescence analyzer (*Thermo Environmental Instruments (TEI), Model 42i*) with a
10 range of 0-200 ppbv and a lower detection limit of 0.40 ppbv. O₃ was monitored with a
11 commercial UV photometric analyzer (*TEI, Model 49i*) with a range of 0-0.050 to 200 ppm
12 and a lower detection limit of 1.0 ppbv. SO₂ was measured using a pulsed UV fluorescence
13 approach (*TEI, Model 43S*). CO was measured by a gas filter correlation, non-dispersive
14 infrared analyzer (*API, Model 300*) with a heated catalytic scrubber to convert CO to CO₂
15 for baseline determination. Quality assurance and control procedures (*e.g.*, instrumental
16 maintenance and calibration) for these devices have been described elsewhere (Guo et al.,
17 2009, 2013). Meteorological parameters, including temperature, relative humidity, solar
18 radiation, wind speed and wind direction, were routinely monitored by a weather station
19 (Vantage Pro 2 plus, Davis Instruments) with a time resolution of 5 minutes. At TC, hourly
20 data of the aforementioned trace gases and meteorological parameters were obtained from the



1 HKEPD (<http://epic.epd.gov.hk/ca/uid/airdata>). Detailed information of the quality assurance
2 and control protocols is available in the HKEPD report (HKEPD, 2015).

3 2.2.2 Sampling and analysis of VOCs

4 Concurrent VOC samples (*i.e.*, non-methane hydrocarbons (NMHCs) and carbonyls) were
5 collected on 21 selected days (including both non-O₃ episodes and O₃ episodes) at both
6 sites. These days were selected on the basis of weather prediction and meteorological data
7 analysis for potentially high and low O₃ days. An O₃ episode day is the day when the peak
8 one-hour averaged O₃ mixing ratio exceeds 100 ppbv (Level II of China National Ambient
9 Air Quality Standard). Please refer to our previous publication for details of this method (Guo
10 et al., 2009).

11 The whole-air samples of NMHCs were collected using 2-L electro-polished stainless steel
12 canisters. The canisters were cleaned, conditioned and evacuated before being used for
13 sampling. A metal bellows pump was used to fill up the canisters with sample air over one-
14 hour integration (with a flow restrictor) to a pressure of 40 psi. Seven one-hour VOC
15 samples (every two hours during 7:00 – 19:00 inclusive) were collected simultaneously at
16 each site. Intensive VOC sampling was also carried out at WS in selected seven days (*i.e.*, 3, 4, 9
17 and 22-25 October) with eleven one-hour samples (every two hours during 1:00 – 22:00
18 inclusive). Totally, 311 valid VOC samples (144 at TC and 167 at WS) were collected in
19 addition to about 5% field blanks and 5% parallel samples for quality assurance purpose. The
20 speciation and abundance of 59 C₂-C₁₁ NMHCs in the canisters were determined by a Model
21 7100 preconcentrator (Entech Instruments Inc., California, USA) coupled with an Agilent
22 5973N gas chromatography-mass selective detector/flame ionization detector (GC-MSD/FID,
23 Agilent Technologies, USA). The detection limit of NMHCs was 3 pptv with a measurement
24 precision of 2-5%, and a measurement accuracy of 5%. Detailed information of the analysis
25 system and quality control and quality assurance for VOC samples can be found elsewhere
26 (Simpson et al., 2010).

27 Carbonyl samples were collected using silica gel filled cartridges impregnated with acidified
28 2,4-dinitrophenylhydrazine (DNPH). Air samples were drawn through the cartridge at a flow
29 rate of 0.8–0.9 L min⁻¹ for 2 hours; the flow rate through the cartridges was monitored with a
30 rotameter which was calibrated before and after each sampling. An O₃ scrubber was
31 connected to the inlet of the DNPH–silica gel cartridge to prevent interference from O₃. In



1 total, 227 carbonyl samples (124 at TC and 103 at WS) were collected with 5 and 6 samples
2 per non-O₃ and O₃ episode day (every two hours during 7:00 - 18:00 inclusive), respectively.
3 All cartridges were stored in a refrigerator at 4 °C after sampling. The sampled carbonyl
4 cartridges were eluted slowly with <5 ml of acetonitrile in the direction opposite to sampling
5 flow into a 5-ml brown volumetric flask, followed by adding acetonitrile to a constant
6 volume of 5 ml. A 20- μ l aliquot was injected into the high performance liquid
7 chromatography (HPLC) system through an auto-sampler. The operating conditions of the
8 HPLC are shown in Table S1. Typically, C₁–C₉ carbonyl compounds were measured
9 efficiently with a detection limit of ~0.2 ppbv.

10 **2.3 Observation-based model (OBM)**

11 A photochemical box model coupled with the Master Chemical Mechanism v3.2 (PBM-
12 MCM) was applied to simulate the O₃ production at WS and TC for the VOC sampling days.
13 The PBM-MCM model is a zero-dimension photochemical box model combined with a near
14 explicit chemical mechanism consisting of 5,900 species and 16,500 reactions, which fully
15 describes the mechanisms of homogeneous reactions in the atmosphere (Jenkin et al., 1997;
16 Jenkin et al., 2003; Saunders et al., 2003). The simulation was constrained by hourly data of
17 meteorological parameters (*i.e.*, temperature and relative humidity) and air pollutants (NO,
18 NO₂, CO, SO₂ and 51 measured VOCs). Since the sampling interval was two hours for each
19 sample, cubic spline interpolation was used to derive VOC concentrations at each hour for
20 modeling purpose. Please see our previous publication for details (Wang et al., 2017a). It is
21 noteworthy that the atmospheric physical processes (*i.e.*, vertical and horizontal transport)
22 were not considered in this model. The PBM-MCM model has been successfully applied in
23 previous studies (Cheng et al., 2010b; Lam et al., 2013; Ling et al., 2014). Details of the
24 model construction can be found in Saunders et al. (2003) and Lam et al. (2013).

25 **2.4 WRF-CMAQ simulation and backward particle release model**

26 In this study, the Weather Research and Forecasting (WRF v3.7.1) model (Skamarock et al.,
27 2008) was used to simulate vertical and horizontal wind fields for various weather systems
28 observed in this campaign, and then provided meteorological parameters required by U.S.
29 EPA Community Multiscale Air Quality (CMAQ v4.7.1) model (www.epa.gov/cmaq).
30 CMAQ is a three-dimensional Eulerian atmospheric chemistry and transport modeling system,
31 which includes complex physical and chemical processes, such as physical transport and
32 diffuse, gas and aqueous chemical transformation, and so on; and it can treat multiple



1 pollutants simultaneously from local to continental scales. A domain system composed of
2 four nested grids (81, 27, 9, 3 km) was adopted to better suit the simulation of mesoscale
3 weather systems, as shown in Figure S1. The domain with finest resolution (3 km) covers the
4 Pearl River Estuary region. Vertically, there were 31 sigma levels for all domains, with the
5 model top fixed at 50 hPa. The major selected physical schemes invoked in WRF and
6 chemical mechanisms used in CMAQ are shown in Table S2. The input meteorological data
7 was made using NCEP FNL (final) data with a horizontal resolution of $1^{\circ} \times 1^{\circ}$
8 (<https://rda.ucar.edu/>). In addition, the geographical data were obtained from the Research
9 Data Archive of National Center for Atmospheric Research (NCAR)
10 (<http://www2.mmm.ucar.edu/wrf/users/downloads.html>). The emission inventories (EI) used
11 in this study included the 2000-based Regional Emission Inventory in ASia (REAS)
12 (Kurokawa et al., 2013) and the 2010-based Multi-resolution Emission Inventory for China
13 (MEIC) (He, 2012), both of which were processed by the Sparse Matrix Operating Kernel
14 Emission (SMOKE) model. The biogenic emissions were calculated by the Model of
15 Emissions of Gases and Aerosols from Nature (MEGAN) (Guenther, 2006). The WRF
16 modelling mainly focused on O₃ episodes with an additional 24hrs' preceding run as spin-up
17 for each episode, and the integration was conducted separately. In addition, the
18 spatiotemporal patterns of CO and O₃ were simulated by WRF-CMAQ during two O₃
19 episodes (see section 3.4). Table S3 gives the index of agreements (IOAs) between the
20 simulated and observed meteorological parameters and air pollutants. Within the range of 0 –
21 1, higher IOAs represent better agreement between the simulated and observed values
22 (Willmott, 1982). Here, IOA was between 0.51 and 0.84 for the simulation of meteorological
23 parameters. Furthermore, it was not lower than 0.50 for primary air pollutants, and reached
24 0.81 for O₃ simulation at both sites. The model performances were comparable to those
25 reported in previous studies (Cabaraban et al., 2013; Wang et al., 2015). Therefore, we
26 accepted the modeling results, in view of the fact that the simulations were only used to
27 qualitatively indicate the interactions between the continental and marine air in this study.

28 Backward particle release simulations were carried out using HYSPLIT model (Stein et al.,
29 2015) for episode days at WS and TC sites during the entire sampling period (Draxler and
30 Rolph, 2003). The backward particle release simulation, which considers the dispersion
31 processes in the atmosphere, is capable of identifying the history of air masses (Guo et al.,
32 2009; Ding et al., 2013a, 2013b). In this work, we applied the model following a method
33 developed by Ding et al. (2013a).



1 3 Results and Discussion

2 3.1 Spatio-temporal variations

3 Table 1 summarizes the meteorological conditions and chemical species observed at WS and
 4 TC. Lower temperature ($25.7 \pm 0.1^\circ\text{C}$) and higher relative humidity ($82.8 \pm 0.4\%$) were
 5 recorded at the marine site (WS) compared to the suburban site (TC) ($p < 0.01$) (temperature:
 6 $26.7 \pm 0.1^\circ\text{C}$ and relative humidity: $67.7 \pm 0.5\%$). At WS, the solar radiation ($635.8 \pm 46.9 \text{ W m}^{-2}$)
 7 was much higher than that at TC ($563.5 \pm 46.1 \text{ W m}^{-2}$, $p < 0.01$), while the average wind speed
 8 at TC ($4.6 \pm 0.1 \text{ m s}^{-1}$) was significantly lower than that measured at WS ($7.2 \pm 0.2 \text{ m s}^{-1}$). The
 9 lower wind speed at TC was related to the roughness of underlying surfaces. However, no
 10 statistical differences were found for the average wind direction (about 81° , northeast wind)
 11 at the two sites, indicating that the two sites were probably under the influence of similar air
 12 masses in most cases.

13 The NO, NO₂, CO, SO₂ and total VOCs (the sum of NMHCs and carbonyls) had lower
 14 average and maximum mixing ratios at WS than those at TC. The lower levels of primary air
 15 pollutants at WS were likely the results of fewer local emission sources, faster photochemical
 16 consumption (as discussed later) and/or more favorable dispersion conditions (*e.g.*, higher
 17 wind speed). In contrast, O₃ was much higher at WS (Table 1), attributable to the
 18 enhancements by both meteorological and photochemical effects, as discussed in sections 3.2
 19 and 3.3.

20 **Table 1.** Descriptive statistics of meteorological parameters and trace gases at the two sites
 21 during the sampling period.

Parameter	WS		TC	
	<i>Mean ± 95% C.I.</i>	<i>Max.</i>	<i>Mean ± 95% C.I.</i>	<i>Max.</i>
Temperature ($^\circ\text{C}$)	25.7 ± 0.1	32.8	26.7 ± 0.1	35.4
Relative humidity (%)	82.8 ± 0.4	98.9	67.7 ± 0.5	96.8
Solar radiation (W m^{-2})*	635.8 ± 46.9	1026.8	563.5 ± 46.1	910.0
Wind speed (m s^{-1})	7.2 ± 0.2	23.8	4.6 ± 0.1	13.8
Wind direction ($^\circ$)	81.3	-	80.9	-
O ₃ (ppbv)	51.3 ± 1.2	173.0	30.0 ± 1.0	159.9
NO (ppbv)	0.7 ± 0.1	21.0	14.0 ± 0.8	115.7



NO ₂ (ppbv)	4.3±0.3	49.3	25.0±0.6	104.2
CO (ppbv)	251.4±6.5	727.7	560.5±6.3	1047.9
SO ₂ (ppbv)	2.4±0.1	12.2	5.9±0.1	19.1
NMHCs (ppbv)	12.7±1.1	32.9	17.7±1.7	60.0
Carbonyls (ppbv)	7.9±0.7	16.3	9.2±0.7	26.5

1 * Average of the daily maximum solar radiation. *C.I.* denotes confidence interval.

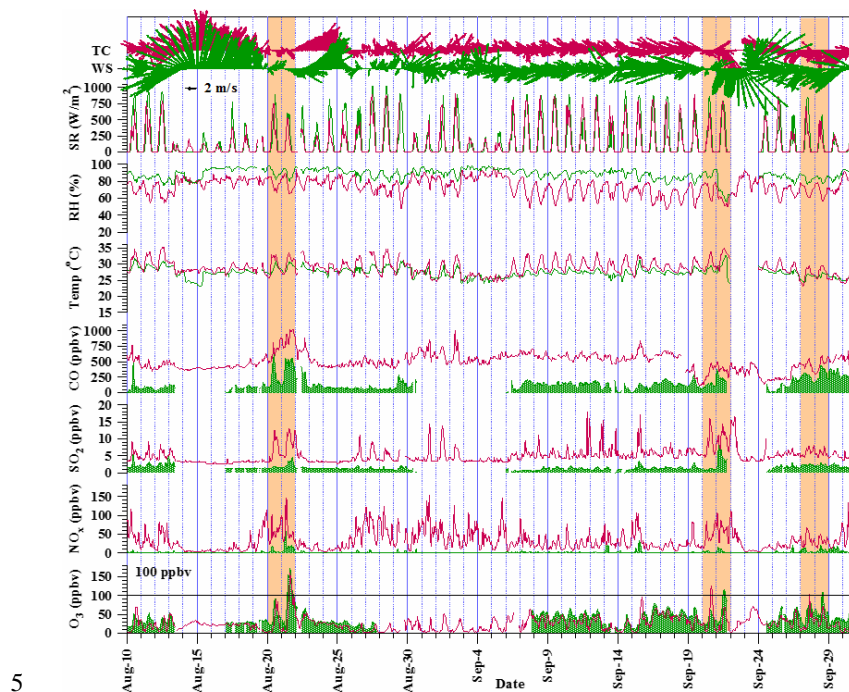
2

3 Time series of local meteorological parameters and hourly mixing ratios of air pollutants at
4 the two sites are illustrated in Figures 2a-2b. The temporal patterns of wind directions were
5 generally similar at both sites, with the dominance of the southerly winds in August and
6 northeastern winds between September and November. Occasionally, the northwesterly
7 winds from the PRD region were observed.

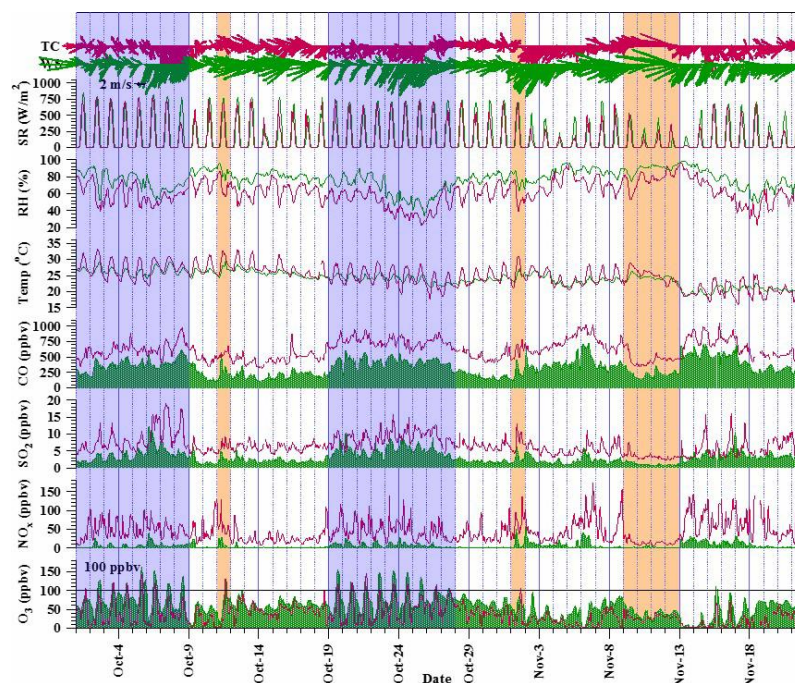
8 This sampling campaign witnessed 17 O₃ episodes and 7 near-O₃ episode days at TC, which
9 refers to the days with maximum hourly mixing ratio of O₃ higher than 100 ppbv and within
10 the range of 80-100 ppbv, respectively. (80 ppbv was Level I of China National Ambient Air
11 Quality Standard for O₃). At WS, 21 O₃ episodes and 6 near-O₃ episodes were recorded.
12 Specifically, 13 O₃ episode days were simultaneously observed at the two sites, with the rest
13 occurred exclusively at one site. On one hand, the primary air pollutants (CO, SO₂ and NO_x)
14 generally increased during O₃ episodes, implying enhanced O₃ formation potentials from the
15 precursors. On the other hand, O₃ episodes were always accompanied by the synoptic
16 conditions, *i.e.*, tropical cyclone (typhoon in the mature form) and continental anticyclone,
17 and/or mesoscale circulations such as SLB, as detailed in Table S4. For example, the two
18 multi-day O₃ episode events, *i.e.*, 1-8 Oct. and 19-27 Oct. (highlighted in blue in Figure 2),
19 were strongly associated with continental high pressure. These episode days generally had
20 high temperature, northerly winds, and intensive solar radiation, with air flows largely from
21 the inland or the coastal areas. Also, the mixing ratios of CO, NO₂ and SO₂ usually increased
22 during these days, suggesting the accumulation of local air pollutants and/or the increasing
23 contribution from regional transport. In contrast, O₃ episodes under the influence of tropical
24 cyclones (highlighted in orange in Figure 2) featured high temperature, strong solar radiation
25 and typically calm or moderate northwesterly to northeasterly winds, except for typhoon



- 1 “Haiyan” occurred on 9-12 Nov. (discussed in section 3.2.1). These conditions were all
- 2 conducive to the formation and accumulation of O₃. Additionally, SLB was also an important
- 3 factor regulating O₃ pollution in this region during O₃ episodes (Table S4). Detailed
- 4 discussions can be found in section 3.2.3.



- 5
- 6 **Figure 2a.** Time series of trace gases and meteorological parameters observed for the
- 7 sampling period of 10 Aug. - 30 Sept. at WS (green) and TC (red). The black line of 100 ppbv
- 8 is the threshold for O₃ episode definition. The dates seriously affected by continental high
- 9 pressure and tropical cyclones are shaded in blue and orange, respectively. Note that there are
- 10 some data missing in these months due to extremely bad weather conditions and instrumental
- 11 failure.
- 12



1

2 **Figure 2b.** Time series of trace gases and meteorological parameters observed for the
3 sampling period of 1 Oct. - 21 Nov at WS (green) and TC (red). The black line of 100 ppbv is
4 the threshold for O₃ episode definition. The dates seriously affected by continental high
5 pressure and tropical cyclones are shaded in red and orange, respectively.

6

7 **3.2 Meteorological influence on O₃ mixing ratios**

8 Descriptive statistics of meteorological parameters during O₃ episode and non-episode days
9 are summarized in Table 2. On episode days the wind speed and relative humidity were lower
10 whereas solar radiation was stronger at both sites, suggesting that this type of weather
11 condition was conducive to the formation and accumulation of tropospheric O₃. Furthermore,
12 the wind direction during non-episodes was predominantly from the east (SCS), while on
13 episodes the winds mainly came from the north and northeast which might bring more
14 pollutants from the urban areas of Hong Kong and inland PRD to the sampling sites. The
15 characteristics of O₃ pollution under different weather conditions were discussed below.

16



1 **Table 2.** Descriptive statistics (Mean \pm 95% C.I.) of meteorological parameters at the two sites
2 during O₃ episodes and non-O₃ episodes days.

Parameter	WS		TC	
	<i>O₃ episode</i>	<i>Non-O₃ episode</i>	<i>O₃ episode</i>	<i>Non-O₃ episode</i>
Temperature (°C)	25.3 \pm 0.2	25.8 \pm 0.1	26.3 \pm 0.3	26.8 \pm 0.2
Wind speed (m s⁻¹)	5.3 \pm 0.2	7.7 \pm 0.2	3.7 \pm 0.2	4.8 \pm 0.1
Wind direction (°)	45.1	89.1	19.5	86.8
Relative humidity (%)	71.7 \pm 1.2	85.7 \pm 0.4	58.4 \pm 1.4	69.6 \pm 0.6
Solar radiation (W m⁻²)*	723.2 \pm 26.1	613.7 \pm 57.6	699.0 \pm 29.1	537.0 \pm 53.1

3 * Average of the daily maximum solar radiation. *C.I.* denotes confidence interval.

4

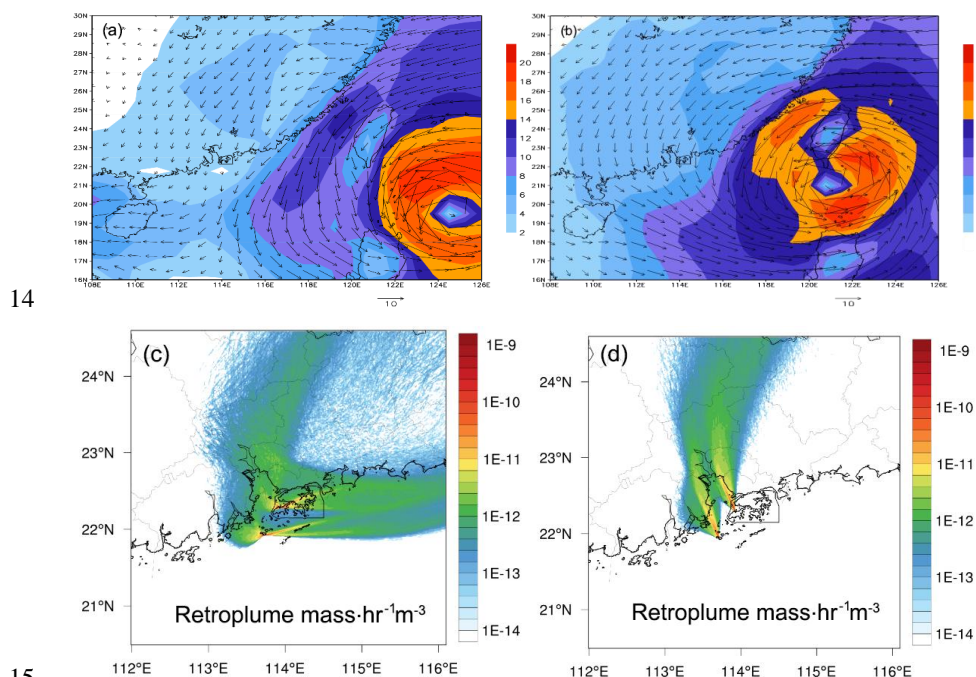
5 3.2.1 Tropical cyclones

6 Tropical cyclone (low-pressure system) is one of the main meteorological conditions
7 conducive to the occurrence of O₃ episodes in Hong Kong (Yin, 2004; Ling et al., 2013). In
8 this study, 7 episode days and 3 near-episode days were closely associated with 5 tropical
9 cyclones (*i.e.*, Trami, Usagi, Wutip, Nari and Krosa) (Table S4 and Figure S2). For example,
10 Trami caused the worst O₃ episode on 21 Aug. with the highest peak hourly O₃ mixing ratios
11 of 160 and 173 ppbv at TC and WS, respectively. These episode or near-episode days usually
12 appeared 1-2 days before the arrival of the tropical cyclones, because the large-scale
13 peripheral subsidence of the tropical cyclones usually creates the meteorological conditions
14 favorable to the formation and accumulation of O₃, such as inversion layer, high temperature,
15 low humidity, intensive light, and weak winds (Wang et al., 1998; Yin, 2004). The tropical
16 cyclones also cause anti-clockwise air flows at their outskirts affecting the wind directions and
17 subsequent the regional transport of air pollution. Figure 3 illustrates surface wind fields and
18 air movement two days (*i.e.*, 20-21 Sept.) before the occurrence of Usagi as an example. It
19 can be seen that when Usagi approached southeastern area of Hong Kong, it led to weak
20 northeasterly and later northwesterly winds which potentially delivered O₃ and its precursors
21 from highly polluted inland PRD region to the sampling sites (Yin, 2004; Wei et al., 2016;
22 Wang et al., 2017a). The wind speed was lower than 4 m s⁻¹ at the sampling sites and in their
23 surrounding area on 20 Sept. (Figure 3a), and it gradually increased on the next day (21 Sept.)



1 with the approaching of the tropical cyclone (Figure 3b). It is noteworthy that the rarely
2 occurred westerly and northwesterly winds caused tropical cyclones resulted in
3 unsynchronized occurrence of O₃ episodes between the two sites (Figures 3c & d). Namely,
4 high O₃ values were observed at TC only on 20 Sept., while O₃ started to increase at WS on
5 the next day (21 Sept.). This discrepancy might indicate the transport of O₃ and/or its
6 precursors from terrestrial area to the offshore site driven by tropical cyclone.

7 Please note, not all tropical cyclones would cause high levels of O₃. For example, the tropical
8 cyclone Haiyan observed on 9-12 Nov. over the SCS did not cause high O₃ levels (Figure 2b).
9 Because the origin of Haiyan was at a lower latitude (southern Guam) and it moved on the
10 waters southwest of PRD (Figure S2), the anti-clockwise air flow caused easterly and
11 southeasterly winds in the north and northeast outer band of Haiyan. The winds originated
12 from SCS brought in clean marine air to the sampling sites, resulting in dilution and
13 dispersion of local air pollutants.



15
16 **Figure 3.** Model simulated 10 m wind vectors (arrows) and wind speed (shaded, unit: m s⁻¹),
17 and the distribution of air mass concentrations (unit: mass hr⁻¹ m⁻³) within surface 100 m
18 simulated by HYSPLIT Lagrangian backward particle release model with WS and TC as the



1 starting points two days (20 Sept. 2013) before (a, c) and one day (21 Sept. 2013) before (b, d)
2 the arrival of Usagi.

3

4 3.2.2 Continental anticyclones

5 In addition to tropical cyclones, the continental anticyclone (high-pressure system) was
6 frequently observed in the region, which often caused high O₃ concentrations. For example,
7 two multi-day O₃ episodes (1-8 Oct. and 19-27 Oct.) occurred at the sampling sites when
8 there were intensive continental anticyclones and weak Western Pacific Subtropical High
9 (WPSH) to the north of Hong Kong (see Figure S3 as examples).

10 The main feature of the anticyclones is sinking air at the center with gentle clockwise winds
11 in the northern hemisphere. The air warms up as it sinks by compression leading to warm,
12 cloudless and dry weather, which is conducive to intensive photochemical O₃ formation. In
13 addition, anticyclone is a large-scale weather system which produces long-lasting settled and
14 calm weather for many days or weeks favorable to the accumulation of primary and
15 secondary pollutants.

16 Indeed, the two continental high pressure systems observed in this campaign lasted 8 and 9
17 days, respectively, with the presence of SLBs occasionally (*i.e.*, 2-5 Oct. and 19-21 Oct.) on
18 the first several days when the synoptic winds were relatively weak. The clockwise and slow
19 movement of the air masses caused northeasterly and easterly winds to the sampling sites and
20 brought in densely polluted air from the inland (Figure 2b) to the coastal areas of the SCS.
21 For example, the CO mixing ratios were significantly elevated during these episode days,
22 with an average of 409 and 683 ppbv at WS and TC, respectively, which were higher than
23 other episode days. The continuous input of exotic air pollutants provided essential “fuel” to
24 local photochemical production of O₃, leading to the severe multi-day O₃ episodes.

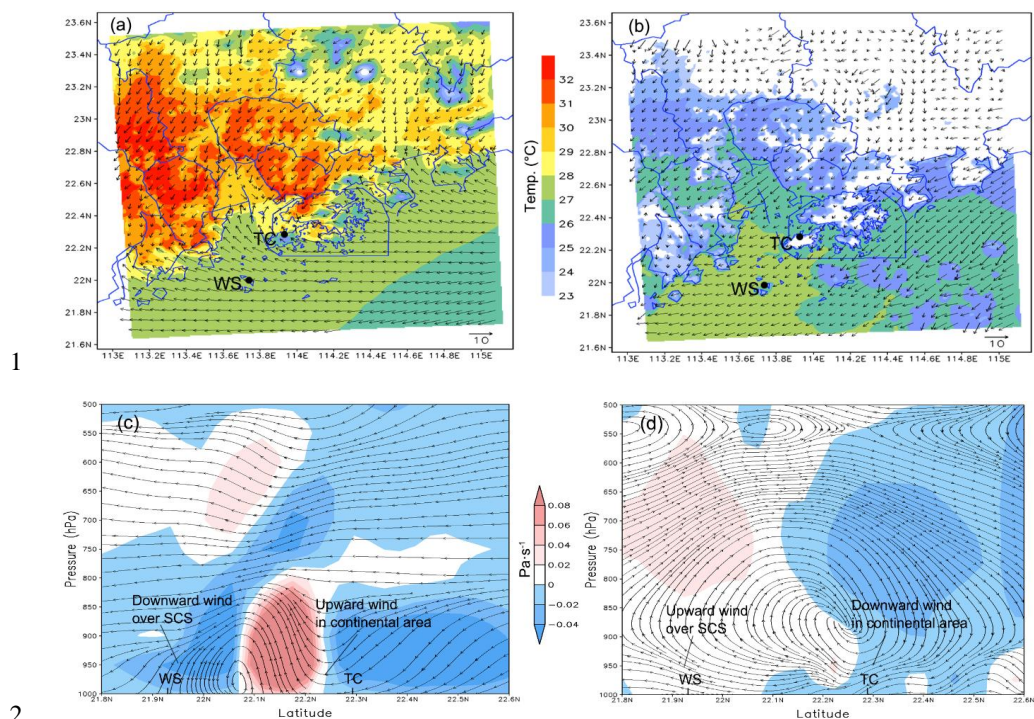
25 3.2.3 Sea-land breeze (SLB) circulation

26 During the sampling period, SLB circulations in the study area were identified on 21 out of
27 104 sampling days. The occurrence frequency was comparable to that reported by Zhang and
28 Zhang (1997) who discovered 70 SLB days in a year in the same region. In this study, 12 O₃
29 episode days were thought to be influenced by SLB (see Table S4), with 5 of them (27-28
30 Sept., 11-12 Oct. and 1 Nov.) under the dominance of tropical cyclones (*i.e.*, Wutip, Nari and
31 Krosa) and the other 7 days in association with the continental anticyclones. In addition to the



1 effects of tropical cyclones and continental anticyclones discussed above, SLB also posed
2 non-negligible impact on O₃ pollution in these cases.

3 SLB circulation is driven by sea-land thermal difference and topographic conditions, and
4 usually happens when the synoptic winds are weak (Liu et al., 2002; Lo et al., 2006; Lu et al.,
5 2009b). In general, the temperature difference between the sea and the land is large on the
6 SLB days. Taking 3 Oct. as an example, the maximum hourly temperature at TC was 3.2 °C
7 higher than that at WS during daytime hours, whereas the minimum hourly temperature in the
8 evening was 2.7 °C lower at TC than at WS. On a typical SLB day, wind blows onshore
9 during the day (sea breeze) and offshore in the evening (land breeze). However, the transition
10 time of breezes in this study was found to vary in a wide range. The sea breeze switched to
11 land breeze between 00:00 and 08:00 with a median of 03:00 for breeze shifting, and 11:00 –
12 18:00 with the median of 14:00 was the time when land breeze turned to sea breeze. Ding et
13 al. (2004) also reported this phenomenon and pointed out that the start time of sea breezes in
14 Hong Kong was generally delayed to noontime due to the synoptic northerly winds blowing
15 from the continental areas to SCS, particularly on O₃ episode days when northerly winds
16 dominated in Hong Kong. For example, the sea breeze commenced at 15:00 on 3 Oct. and
17 transited to land breeze at 4:00 on 4 Oct. (Figure 4). Figures 4a and 4b depict the surface
18 wind fields with a sea breeze and a land breeze, respectively. The vertical wind fields with
19 the sea breeze and land breeze are presented in Figures 4c and 4d, respectively. Surface and
20 vertical SLB circulations were clearly seen in these panels of Figure 4. The mesoscale
21 circulations caused by SLB might promote the interactions between the continental (TC) and
22 marine (WS) atmospheres. Specifically, the primary air pollutants observed at TC could be
23 transported to WS by land breeze. Moreover, the air masses could return to TC after
24 sufficient photochemical evolutions over SCS, during which O₃ might also be elevated in the
25 continental areas.



1

2

3

4

5

6

7

8

9

10

11

12

13

14

15

16

17

Figure 4. SLB circulation on 3-4 Oct. 2013, showing surface wind pattern (arrows) and temperature (color) at 17:00 on 3 Oct. (a) and at 04:00 on 4 Oct. (b). Vertical cross-section (taken over a longitude of 113.85 °E, mean of the longitudes of TC and WS) depicting the $v-w$ wind stream (arrow) and the index of $\omega * 100$ (color) at 17:00 on 3 Oct. (c); and at 04:00 on 4 Oct. (d). For figures (c) and (d), the blue color (negative) and light red color (positive) present downward and upward winds, respectively. Figures (a) and (c) represent a sea breeze, and Figures (b) and (d) show a land breeze. Note that ω is the vertical velocity in isobaric coordinates.

3.3 Chemical characteristics of air masses

3.3.1 Chemical composition

To inspect the chemical characteristics of air masses on O₃ episode days and non-O₃ episode days, chemical species are statistically summarized at the two sites (Table 3). As expected, the levels of all pollutants (*i.e.*, O₃, NO₂, CO, SO₂, NMHCs and carbonyls) were significantly higher on O₃ episode days for both sites ($p < 0.05$), except for the comparable or even lower



1 NO due to its titration to O₃ (see Section 3.3.2). Table S5 shows the top 10 NMHC species
 2 observed during O₃ episodes and non-episodes at the two sites. The dominant species were
 3 quite similar regardless of episode or non-episode days at both sites. The higher
 4 concentrations of both primary and secondary pollutants on episode days than those on non-
 5 episode days were likely due to more intense photochemical reactions, more local pollutant
 6 accumulation as well as the regional transport of more highly polluted air masses. On the
 7 other hand, the similar NMHCs composition at both sites during both episodes and non-
 8 episodes indicated somewhat interaction of air masses between the two sites regardless of O₃
 9 levels.

10 It is worth to mention that O₃ was much higher at WS than that at TC during both episodes
 11 and non-episodes ($p < 0.01$), with an average difference of 30.2 ppbv and 16.7 ppbv,
 12 respectively (Table 3), though the levels of O₃ precursors (*i.e.*, NO_x and VOCs) at WS were
 13 lower. Insight into VOC ratios found that ethene/ethane (0.5 ± 0.04) and toluene/benzene
 14 (2.2 ± 0.5) at WS were significantly ($p < 0.05$) lower than those at TC (0.7 ± 0.1 and 2.9 ± 0.4 ,
 15 respectively), likely indicating that the air masses at WS were more aged (Guo et al., 2007).
 16 Therefore, the higher O₃ at WS might be partially attributable to the aging of air masses (*e.g.*,
 17 during the transport of continental air).

18 **Table 3.** Descriptive statistics (Mean \pm 95% *C.I.*) of measured air pollutants, simulated OH
 19 and O₃ production rates at the two sites during O₃ episodes and non-O₃ episodes days.

Parameter	WS		TC	
	<i>O₃ episode</i>	<i>Non-O₃ episode</i>	<i>O₃ episode</i>	<i>Non-O₃ episode</i>
O ₃ (ppbv)	74.3 \pm 3.0	43.9 \pm 1.0	44.1 \pm 3.6	27.2 \pm 0.8
O _x (ppbv)	81.6 \pm 2.9	47.8 \pm 1.0	83.3 \pm 3.7	49.4 \pm 1.0
NO (ppbv)	0.6 \pm 0.1	0.7 \pm 0.1	11.5 \pm 1.4	14.5 \pm 0.9
NO ₂ (ppbv)	7.3 \pm 0.6	3.3 \pm 0.3	39.2 \pm 1.7	22.2 \pm 0.6
CO (ppbv)	391.4 \pm 9.1	209.4 \pm 6.8	652.9 \pm 16.0	541.9 \pm 6.5
SO ₂ (ppbv)	4.3 \pm 0.2	1.9 \pm 0.1	8.1 \pm 0.3	5.5 \pm 0.1
NMHCs (ppbv)	17.7 \pm 1.4	9.6 \pm 1.2	20.2 \pm 2.2	16.8 \pm 2.1
Carbonyls (ppbv)	10.3 \pm 0.8	5.4 \pm 0.4	12.0 \pm 1.3	8.1 \pm 0.7
NO ₂ /NO (ppbv/ppbv)	12.7 \pm 1.1	4.7 \pm 0.5	3.4 \pm 0.4	1.5 \pm 0.2
Simulated OH ($\times 10^6$ molecules cm ⁻³)	5.4 \pm 1.0	3.3 \pm 0.8	1.2 \pm 0.3	1.5 \pm 0.3



1 * Average of the daily maximum solar radiation. *C.I.* denotes confidence interval. $O_x = O_3 + NO_2$.

2

3 3.3.2 Influence of NO titration

4 Apart from the age of air masses, NO titration is another important factor influencing O_3
5 concentration. In areas with high NO levels, the NO titration ($O_3 + NO \rightarrow NO_2 + O_2$) is a
6 main process consuming O_3 . In this study, the average NO mixing ratio at TC was 14.0 ± 0.8
7 ppbv, compared to 0.7 ± 0.1 ppbv at WS (Table 1). The much lower NO at WS implied
8 weaker titration to O_3 , which enabled the survival of O_3 in high concentration. A direct
9 evidence of NO titration effect was the trough of O_3 during the morning rush hours (06:00-
10 07:00), together with an increase of NO_2 (Figure S4). Furthermore, the total oxidants ($O_x =$
11 $O_3 + NO_2$), which are usually adopted to take into account the NO titration influence, were
12 comparable ($p > 0.05$) between TC and WS with mean values of 83.3 ± 3.7 ppbv and 81.6 ± 2.9
13 ppbv during O_3 episodes, and 49.4 ± 1.0 ppbv and 47.8 ± 1.0 ppbv during non-episodes,
14 respectively (Table 3). This was reasonable in view of the interactions between the two sites.
15 However, the remarkably higher O_3 and lower NO at WS indicated that NO titration was a
16 determinant factor regulating the O_3 levels at both sites.

17 Moreover, NO titration is generally more significant on high O_3 days, resulting in higher
18 NO_2/NO ratios due to the conversion of NO to NO_2 by O_3 . Indeed, the mean NO_2/NO ratios
19 increased from 4.7 ± 0.5 at WS and 1.5 ± 0.2 at TC during non-episodes to 12.7 ± 1.1 and
20 3.4 ± 0.4 during O_3 episodes, respectively, implying that more O_3 was titrated by NO during
21 episodes. As a result, NO at TC was lower ($p < 0.01$) during O_3 episodes than during non-
22 episodes (Table 3). It is noteworthy that NO at WS was on the same level between O_3 episode
23 and non- O_3 episode days ($p > 0.05$). This probably related to the weak titration at this marine
24 site due to the trivial NO concentrations in both periods, as well as the counteracting effect of
25 the increased transport of NO under northerly winds against the enhanced titration during O_3
26 episodes.

27 The aforementioned discussion demonstrated that NO titration played an important role in
28 altering O_3 distribution, especially on O_3 episodes days. The lower NO (weaker NO titration)
29 partially resulted in the higher O_3 concentrations observed at WS.



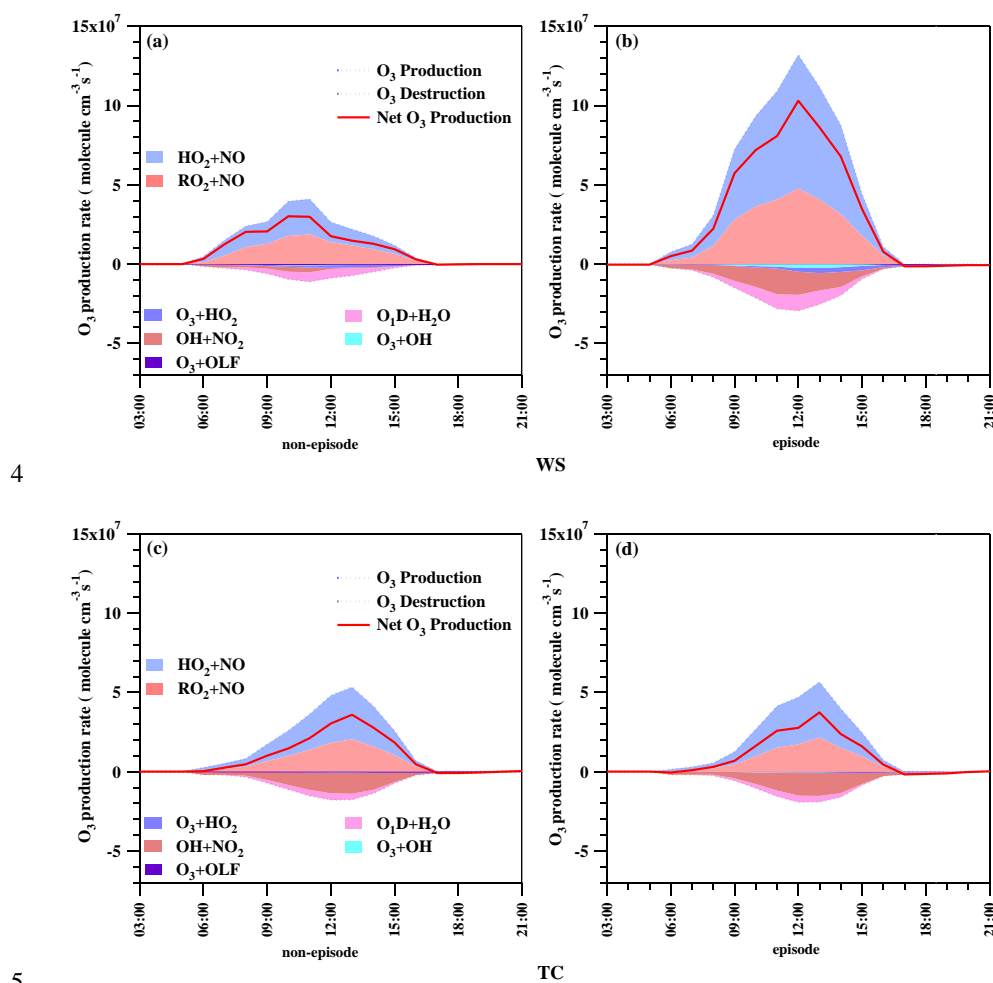
1 3.3.3 Atmospheric oxidative capacity

2 The O₃ formation is generally initiated by the oxidations of VOCs by OH. Furthermore, the
3 oxidative radicals (*e.g.*, RO₂) generated from these reactions experience an array of
4 transformations, through which OH can be recycled. Thus, the OH concentration is an
5 important indicator to evaluate the atmospheric oxidative capacity and the potential of O₃
6 formation. As shown in Table 3, the OH concentration simulated by PBM-MCM model was
7 significantly higher ($p < 0.05$) at WS than that at TC, regardless of O₃ episode ($5.4 \pm 1.0 \times 10^6$
8 molecules cm⁻³) or non-episode days ($3.3 \pm 0.8 \times 10^6$ molecules cm⁻³). This indicated that the
9 oxidative capacity of the atmosphere at WS was stronger than that at TC, which might
10 explain the higher O₃ at WS. Moreover, while the simulated OH remained unchanged
11 ($p > 0.05$) at TC, it increased largely ($p < 0.05$) from non-episodes to episodes at WS,
12 suggesting that the oxidative capacity of the atmosphere at WS was more enhanced during O₃
13 episodes.

14 Furthermore, we simulated the rates of O₃ production, destruction and net O₃ production at
15 both sites, as presented in Figure 5. No significant change in net O₃ production was observed
16 between O₃ episode ($1.1 \pm 0.6 \times 10^7$ molecules cm⁻³ s⁻¹) and non-episode days ($1.2 \pm 0.3 \times 10^7$
17 molecules cm⁻³ s⁻¹) at TC ($p > 0.05$). Since previous studies (Cheng et al., 2010a; Wang et al.,
18 2017a) repeatedly confirmed that O₃ formation at TC was limited by VOCs, the unchanged
19 net O₃ production might be due to the balance between the increased O₃ production and O₃
20 destruction resulting from the elevated VOCs and NO_x during O₃ episodes, respectively. On
21 the contrary, the net O₃ production increased remarkably from non-episodes ($1.2 \pm 0.2 \times 10^7$
22 molecules cm⁻³ s⁻¹) to O₃ episodes ($3.9 \pm 0.8 \times 10^7$ molecules cm⁻³ s⁻¹) at WS. Insight into the O₃
23 formation and destruction pathways found that the slight increases of O₃ destructions (mainly
24 through OH+NO₂ and O¹D+H₂O) were overridden by the great enhancements of O₃
25 productions through RO₂+NO and HO₂+NO. Our recent study (Wang et al., 2017b) revealed
26 that O₃ formation at WS was in a transition regime and much more sensitive to NO_x during
27 non-episodes, when the principal photochemical reaction pathways to produce O₃ (*i.e.*,
28 RO₂+NO and HO₂+NO) were seriously limited by the low NO_x levels. During O₃ episodes,
29 with the increase of NO_x (Table 3), the contributions of the aforementioned two O₃
30 production pathways were significantly enhanced (Figure 5). In addition, the increased VOCs
31 also contributed to the O₃ formation by producing more RO₂ radicals (not shown here)
32 through OH-initiated reactions. Therefore, the combined effect of elevated VOCs and NO_x



- 1 during O₃ episodes at WS was the increase of O₃ production, which was insignificant at TC.
- 2 Detailed discussion on the O₃ photochemistry at WS can be found in our recent publication
- 3 (Wang et al., 2017b).



- 6 **Figure 5.** Simulated rates of O₃ production, destruction, and net O₃ production (unit:
7 molecules cm⁻³ s⁻¹) on O₃ episode and non-episode days at WS (panels (a) and (b)) and TC
8 (panels (c) and (d)). Panels (a) and (b) were adapted from our recent publication (Wang et al.
9 2017b).

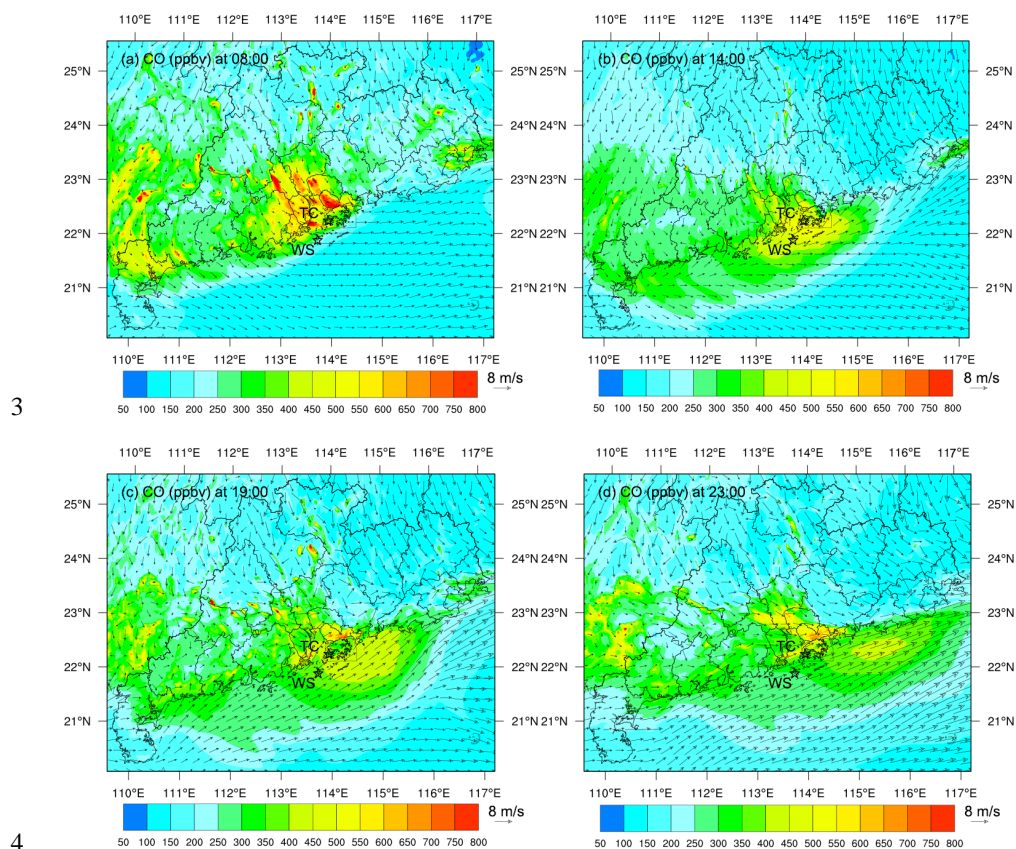


1 3.4 Impact of air mass interaction on O₃ pollution in coastal areas

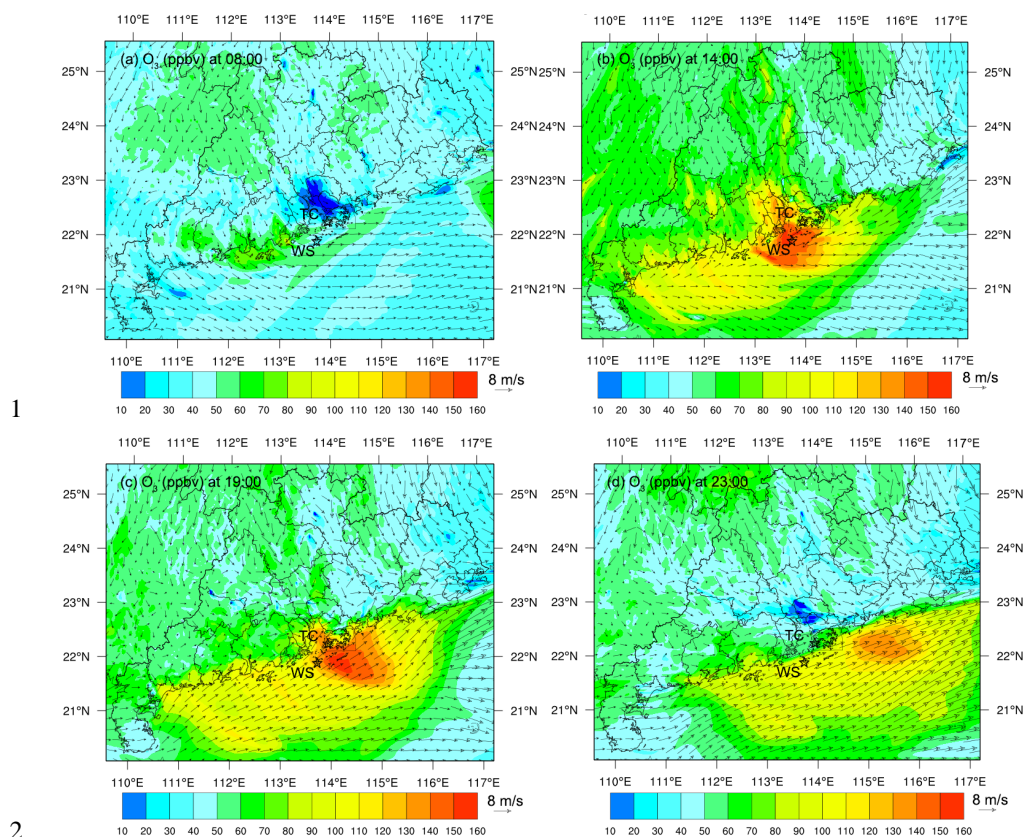
2 Driven by various weather systems (*e.g.*, continental anticyclones, WPSH, tropical cyclones
3 and SLBs), continental and marine air masses frequently interact with each other in the
4 coastal areas. When continental air masses intrude into marine atmosphere, the chemical
5 composition and atmospheric oxidative capacity over the marine atmosphere will be altered
6 by the introduction of anthropogenic pollutants. Taken 21 Aug. as an example, when the
7 sampling sites (TC and WS) were under northwesterly to southwesterly winds caused by
8 tropical cyclone (Figure 2a), the maximum hourly O₃ reached 160 and 173 ppbv at TC and
9 WS, respectively. Correspondingly, the primary air pollutants all stayed on high levels,
10 compared to those during non-episodes (Figure 2a). Since WS was almost free of
11 anthropogenic emissions, the great abundances of both primary and secondary air pollutants
12 implied the influence of continental pollution on air quality at this site. Figures 6-7 depict the
13 spatial distributions of CO and O₃ over the region of interest at selective time (08:00, 14:00,
14 19:00 and 23:00) on 21 Aug., respectively. CO is presented as an example of primary air
15 pollutants emitted from anthropogenic sources. The spatiotemporal patterns of CO and O₃
16 were simulated by WRF-CMAQ. Noticeably, the model well reproduced high level of CO in
17 PRD region at 08:00, which was reasonable in view of the vehicular emissions in urban areas
18 during morning rush hours. However, under the dominance of northwesterly winds in the
19 morning, the center of high CO moved to the coastal areas. Even though the winds changed
20 to southwesterly at noon, CO concentration over SCS was still remarkably elevated according
21 to the simulated results at 14:00. Further, the spatial distribution of CO at 19:00 and 23:00
22 confirmed the continuous movement of the polluted air masses away from the land under
23 southwesterly winds. It should be noted that the increase of CO in PRD region at 19:00 and
24 23:00 were most likely caused by the vehicle emissions during evening rush hours. Overall,
25 the dynamic distribution of CO in the study area clearly indicated the interaction between
26 continental and marine atmospheres. As a result of the intrusion of continental air, high level
27 of O₃ was simulated over SCS at 14:00 (Figure 7b), which was comparable to the observed
28 value (148 ppbv) at WS. Moreover, O₃ was even higher over SCS than that in continental
29 area, due mainly to the more aged air masses, lower NO titration and higher oxidative
30 capacity of the atmosphere (see section 3.3). Consistent with CO, the center of high O₃
31 moved away from the land. At 19:00, the O₃-laden air mass penetrated into the SCS ~300 km,
32 causing ~8,000 km² water area (8 times the area of Hong Kong) under high level of O₃ (>100



- 1 ppbv). This case provided solid evidence of the transport of continental air masses to SCS,
- 2 which aggravated air pollution (particularly O₃ pollution) in this offshore area.



5 **Figure 6.** Spatial distribution of CO at 08:00 (a), 14:00 (b), 19:00 (c) and 23:00 (d) on 21
6 August simulated by WRF-CMAQ, taken as an example of the “Outflow” interaction pattern.
7 Arrows in the figure represent the surface wind field.



1

2

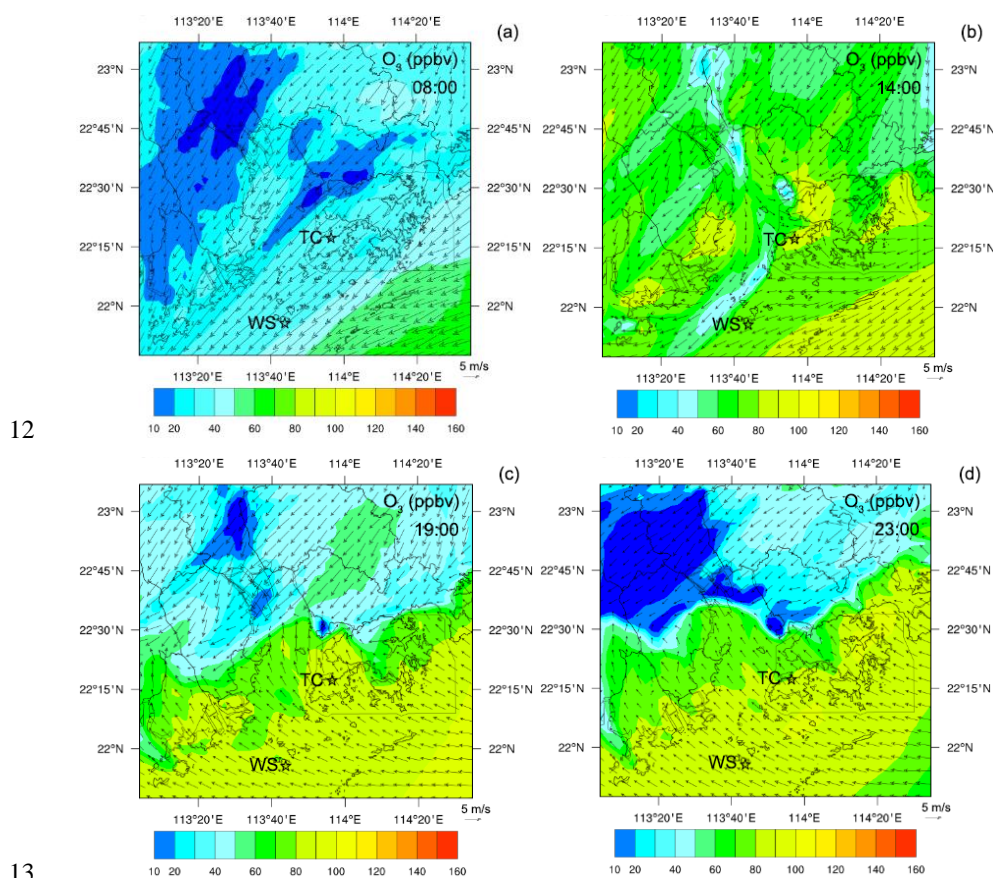
3 **Figure 7** Spatial distribution of O₃ at 08:00 (a), 14:00 (b), 19:00 (c) and 23:00 (d) on 21
4 August simulated by WRF-CMAQ, taken as an example of the “Outflow” interaction pattern.
5 Arrows in the figure represent the surface wind field.

6

7 In contrast to outflow of continental air masses, the continental area near the coast could also
8 be immersed by oceanic air under sea breeze. Contrary to our general expectation that ocean
9 airflow dilutes air pollution, the sea breeze carrying elevated O₃ formed over SCS might
10 build up the terrestrial O₃ in the coastal area in some cases. Figure 8 shows the spatial
11 distribution of O₃ over the study area on 3 Oct., as an example of SLB regulating O₃
12 formation and distribution (see Figure 4). Similar to the aforementioned scenario controlled
13 by tropical cyclone, the simulated O₃ at 14:00 was generally higher over SCS than in the
14 terrestrial area, indicating the transport of polluted air masses from the land to the sea area.
15 This was confirmed by the prevailing northeasterly winds in the morning (08:00 here).
16 However, the O₃-laden air did not move far away from the land subsequently. Instead, it
17 progressively approached the land, leading to increase of O₃ concentration in most parts of



1 Hong Kong. This is because the wind direction in the coastal region changed from
2 northeasterly to southeasterly at 17:00. Namely, the sea breeze appeared in late afternoon,
3 which delivered the high O_3 formed over SCS to the continental areas near the coast. In fact,
4 the air quality monitoring stations deployed in southern Hong Kong by HKEPD also recorded
5 the O_3 peak in the evening when O_3 could not be formed locally (Figure S5), further
6 confirming the recirculation of O_3 -laden air from SCS to coastal areas of Hong Kong under
7 sea-breeze. However, the oceanic air did not penetrate further into the inland PRD, which
8 was likely stopped by the strong northeasterly winds dominated in the inland areas. Overall, it
9 can be seen that SLB as a common interaction between marine and continental atmospheres
10 played important role in regulating O_3 formation and distribution in coastal region of SCS,
11 which is also applicable to other similar mesoscale environments over the world.





1 **Figure 8.** Spatial distribution of O_3 at 08:00 (a), 14:00 (b), 19:00 (c) and 23:00 (d) on 3
2 October, taken as an example of the “SLB” interaction pattern. Arrows in the figure represent
3 the surface wind field.

4

5 **4. Conclusions**

6 Coastal regions with dense population, economic prosperity and environmental pollution are
7 common in the world. This study provided an overview of O_3 pollution in warm seasons
8 around a coastal region of SCS, focusing on the influences of interactions between marine
9 and continental atmospheres on air quality in this subtropical region. The concurrent
10 measurements of primary and secondary air pollutants at TC (a continental site) and WS (a
11 marine site) from August to November 2013 indicated that O_3 was much higher at WS than
12 that at TC, contrary to the more abundant primary air pollutants at TC. At the two sites, O_3
13 episodes and near- O_3 episodes were frequently observed, which were closely associated with
14 continental anticyclone, tropical cyclone and SLB. In addition to high temperature, strong
15 solar radiation and weak wind, the aforementioned meteorological conditions all favored the
16 transport of polluted air masses from continental areas to SCS, during which the air pollutants
17 were transformed with the aging of air masses. After arriving in SCS, the land-originated air
18 pollutants further involved in intensive photochemical reactions with the trait of low NO
19 titration to O_3 and high O_3 production rate, leading to higher O_3 level in marine atmosphere
20 (WS) than that in coastal cities (TC). In addition to the continental outflow that aggravated O_3
21 pollution over SCS, SLB as a common interaction in coastal areas also often facilitated the
22 recirculation of O_3 formed over SCS to the continental areas, building up O_3 concentration in
23 coastal cities under sea breeze. The findings can be extended to other similar regions to
24 advance our understanding of O_3 pollution.

25 **Acknowledgements**

26 This project was supported by the Natural Science Foundation of China (Grant No.
27 41275122), the Research Grants Council (RGC) of the Hong Kong Government of Special
28 Administrative Region (PolyU5154/13E, PolyU152052/14E, PolyU152052/16E and
29 CRF/C5004-15E), the Guangdong special fund for science and technology development
30 (2017B020216007), and partly by the Hong Kong PolyU internal grant (G-SB63, 1-BBW4
31 and 4-ZZFW). The authors thank HKEPD for provision of the air quality and meteorological
32 data at TC site, and are grateful to Po On Commercial Association Wan Ho Kan Primary



1 School at Tung Chung and the National Marine Environmental Monitoring Station at
2 Wanshan Island for their generous support on the field study. Contributions to field
3 measurements by Kalam Cheung, Dawei Wang, Bo Liu, Nan Wang, Jiamin Ou, Huanghuang
4 Yan and Xiaoxin Fu are also highly appreciated. The authors also gratefully acknowledge the
5 NOAA Air Resources Laboratory (ARL) for the provision of the HYSPLIT transport and
6 dispersion model and/or READY website (<http://www.ready.noaa.gov>) used in this
7 publication.

8 **References**

- 9 Adame, J. A., Serrano, E., Bolívar, J. P., and de la Morena, B. A.: On the Tropospheric
10 Ozone Variations in a Coastal Area of Southwestern Europe under a Mesoscale Circulation,
11 *Journal of Applied Meteorology and Climatology*, 49, 748-759, 10.1175/2009jamc2097.1,
12 2010.
- 13 Bell, M. L., Goldberg, R., Hogrefe, C., Kinney, P. L., Knowlton, K., Lynn, B., Rosenthal, J.,
14 Rosenzweig, C., and Patz, J. A.: Climate change, ambient ozone, and health in 50 US cities,
15 *Climatic Change*, 82(1-2), 61-76, 2007.
- 16 Cabaraban, M. T. I., Kroll, C. N., Hirabayashi, S., and Nowak, D. J.: Modeling of air
17 pollutant removal by dry deposition to urban trees using a WRF/CMAQ/i-Tree Eco coupled
18 system, *Environmental pollution*, 176, 123-133, 2013.
- 19 Chan, C. Y.: Effects of Asian air pollution transport and photochemistry on carbon monoxide
20 variability and ozone production in subtropical coastal south China, *Journal of Geophysical*
21 *Research*, 107, 10.1029/2002jd002131, 2002.
- 22 Cheng, H., Guo, H., Saunders, S., Lam, S., Jiang, F., Wang, X., Simpson, I., Blake, D., Louie,
23 P., and Wang, T.: Assessing photochemical ozone formation in the Pearl River Delta with a
24 photochemical trajectory model, *Atmospheric Environment*, 44, 4199-4208, 2010b.
- 25 Cheng, H., Guo, H., Wang, X., Saunders, S. M., Lam, S. H. M., Jiang, F., Wang, T., Ding, A.,
26 Lee, S., and Ho, K.: On the relationship between ozone and its precursors in the Pearl River
27 Delta: application of an observation-based model (OBM), *Environmental Science and*
28 *Pollution Research*, 17, 547-560, 2010a.
- 29 Cui, J., Deolal, S. P., Sprenger, M., Henne, S., Staehelin, J., Steinbacher, M., and Nedelec, P.:
30 Free tropospheric ozone changes over Europe as observed at Jungfraujoch (1990-2008): An



- 1 analysis based on backward trajectories, *Journal of Geophysical Research - Atmospheres*,
2 116, 2011.
- 3 Derwent, R. G., Manning, A. J., Simmonds, P. G., Spain, T. G., and O'Doherty, S.: Analysis
4 and interpretation of 25 years of ozone observations at the Mace Head Atmospheric Research
5 Station on the Atlantic Ocean coast of Ireland from 1987 to 2012, *Atmospheric Environment*,
6 80, 361-368, [10.1016/j.atmosenv.2013.08.003](https://doi.org/10.1016/j.atmosenv.2013.08.003), 2013.
- 7 Ding, A. J., Wang, T., Zhao, M., Wang, T. J., and Li, Z. K.: Simulation of sea-land breezes
8 and a discussion of their implications on the transport of air pollution during a multi-day
9 ozone episode in the Pearl River Delta of China, *Atmospheric Environment*, 38, 6737-6750,
10 [10.1016/j.atmosenv.2004.09.017](https://doi.org/10.1016/j.atmosenv.2004.09.017), 2004.
- 11 Ding, A. J., Wang, T., Thouret, V., Cammas, J. P., and Nedelec, P.: Tropospheric ozone
12 climatology over Beijing: analysis of aircraft data from the MOZAIC program, *Atmospheric
13 Chemistry and Physics*, 8, 1-13, 2008.
- 14 Ding, A. J., Fu, C. B., Yang, X. Q., Sun, J. N., Zheng, L. F., Xie, Y. N., Herrmann, E., Nie,
15 W., Petäjä T., Kerminen, V. M., and Kulmala, M.: Ozone and fine particle in the western
16 Yangtze River Delta: An overview of 1 yr data at the SORPES station, *Atmospheric
17 Chemistry and Physics*, 13, 5813-5830, [10.5194/acp-13-5813-2013](https://doi.org/10.5194/acp-13-5813-2013), 2013b.
- 18 Ding, A. J., Wang, T., and Fu, C. B.: Transport characteristics and origins of carbon
19 monoxide and ozone in Hong Kong, South China, *Journal of Geophysical Research -
20 Atmospheres*, 118, 9475-9488, 2013a.
- 21 Draxler, R. R., and Rolph, G. D.: HYSPLIT (HYbrid Single-Particle Lagrangian Integrated
22 Trajectory) Model access via NOAA ARL READY Website
23 (<http://www.arl.noaa.gov/ready/hysplit4.html>). , NOAA Air Resources Laboratory, Silver
24 Spring, Maryland, USA, 2003.
- 25 Fowler, D., Pilegaard, K., Sutton, M. A., Ambus, P., Raivonen, M., Duyzer, J., Simpson, D.,
26 Fagerli, H., Fuzzi, S., Schjoerring, J. K., Granier, C., Neftel, A., Isaksen, I. S. A., Laj, P.,
27 Maione, M., Monks, P. S., Burkhardt, J., Daemmgen, U., Neiryneck, J., Personne, E.,
28 Wichink-Kruit, R., Butterbach-Bahl, K., Flechard, C., Tuovinen, J. P., Coyle, M., Gerosa, G.,
29 Loubet, B., Altimir, N., Gruenhage, L., Ammann, C., Cieslik, S., Paoletti, E., Mikkelsen, T.
30 N., Ro-Poulsen, H., Cellier, P., Cape, J. N., Horvath, L., Loreto, F., Niinemets, U., Palmer, P.
31 I., Rinne, J., Misztal, P., Nemitz, E., Nilsson, D., Pryor, S., Gallagher, M. W., Vesala, T.,



- 1 Skiba, U., Brüeggemann, N., Zechmeister-Boltenstern, S., Williams, J., O'Dowd, C., Facchini,
2 M. C., de Leeuw, G., Flossman, A., Chaumerliac, N., and Erisman, J. W.: Atmospheric
3 composition change: Ecosystems-Atmosphere interactions, *Atmospheric Environment*, 43,
4 5193-5267, 10.1016/j.atmosenv.2009.07.068, 2009.
- 5 Guenther, C. C.: Estimates of global terrestrial isoprene emissions using MEGAN (Model of
6 Emissions of Gases and Aerosols from Nature), *Atmospheric Chemistry and Physics*, 6,
7 3181-3210, 2006.
- 8 Guo, H., Jiang, F., Cheng, H. R., Simpson, I. J., Wang, X. M., Ding, A. J., Wang, T. J.,
9 Saunders, S. M., Wang, T., Lam, S. H. M., Blake, D. R., Zhang, Y. L., and Xie, M.:
10 Concurrent observations of air pollutants at two sites in the Pearl River Delta and the
11 implication of regional transport, *Atmospheric Chemistry and Physics*, 9, 7343-7360, 2009.
- 12 Guo, H., Ling, Z. H., Cheung, K., Jiang, F., Wang, D. W., Simpson, I. J., Barletta, B.,
13 Meinardi, S., Wang, T. J., Wang, X. M., Saunders, S. M., and Blake, D. R.: Characterization
14 of photochemical pollution at different elevations in mountainous areas in Hong Kong,
15 *Atmospheric Chemistry and Physics*, 13, 3881-3898, 10.5194/acp-13-3881-2013, 2013.
- 16 Guo, H., So, K. L., Simpson, I. J., Barletta, B., Meinardi, S., and Blake, D. R.: C₁-C₈ volatile
17 organic compounds in the atmosphere of Hong Kong: Overview of atmospheric processing
18 and source apportionment, *Atmospheric Environment*, 41(7), 1456-1472, 2007.
- 19 HKEPD: Air Quality in Hong Kong 2014, available at:
20 http://www.aqhi.gov.hk/api_history/english/report/files/AQR2014e_Update0616.pdf, Hong
21 Kong Environmental Protection Department, 2015.
- 22 Huang, J. P., Fung, J. C. H., Lau, A. K. H., and Qin, Y.: Numerical simulation and process
23 analysis of typhoon-related ozone episodes in Hong Kong, *Journal of Geophysical Research*,
24 110, 10.1029/2004jd004914, 2005.
- 25 IPCC: Climate Change 2014: Synthesis Report. Contribution of Working Groups I, II and III
26 to the Fifth Assessment Report of the Intergovernmental Panel on Climate Change, [Core
27 Writing Team, R.K. Pachauri and L.A. Meyer (eds.)], IPCC, Geneva, Switzerland, 151, 2014.
- 28 Jenkin, M. E., Saunders, S. M., and Pilling, M. J.: The tropospheric degradation of volatile
29 organic compounds: A protocol for mechanism development, *Atmospheric Environment*, 31,
30 81-104, 1997.



- 1 Jenkin, M. E., Saunders, S. M., Wagner, V., and Pilling, M. J.: Protocol for the development
2 of the Master Chemical Mechanism, MCM v3 (Part B): tropospheric degradation of aromatic
3 volatile organic compounds, *Atmospheric Chemistry and Physics*, 3, 181-193, 2003.
- 4 Jiang, F., Guo, H., Wang, T., Cheng, H., Wang, X., Simpson, I., Ding, A., Saunders, S., Lam,
5 S., and Blake, D.: An ozone episode in the Pearl River Delta: Field observation and model
6 simulation, *Journal of Geophysical Research*, 115, D22305, doi:10.1029/2009JD013583,
7 2010.
- 8 Jiang, Y. C., Zhao, T. L., Liu, J., Xu, X. D., Tan, C. H., Cheng, X. H., Bi, X. Y., Gan, J. B.,
9 You, J. F., and Zhao, S. Z.: Why does surface ozone peak before a typhoon landing in
10 southeast China? *Atmospheric Chemistry and Physics*, 15, 13331-13338, 10.5194/acp-15-
11 13331-2015, 2015.
- 12 He K.: Multi-resolution Emission Inventory for China (MEIC): model framework and 1990-
13 2010 anthropogenic emissions. In AGU Fall Meeting Abstracts 2012 Dec.
- 14 Kumar, P., and Imam, B.: Footprints of air pollution and changing environment on the
15 sustainability of built infrastructure, *Science of the Total Environment*, 444, 85-101,
16 10.1016/j.scitotenv.2012.11.056, 2013.
- 17 Kurokawa, J., Ohara, T., Morikawa, T., Hanayama, S., Janssens-Maenhout, G., Fukui, T.,
18 Kawashima, K., and Akimoto, H.: Emissions of air pollutants and greenhouse gases over
19 Asian regions during 2000–2008: Regional Emission inventory in ASia (REAS) version 2,
20 *Atmospheric Chemistry and Physics*, 13(21), 11019-11058, 2013.
- 21 Lam, S. H. M., Saunders, S. M., Guo, H., Ling, Z. H., Jiang, F., Wang, X. M., and Wang, T.
22 J.: Modelling VOC source impacts on high ozone episode days observed at a mountain
23 summit in Hong Kong under the influence of mountain-valley breezes, *Atmospheric*
24 *Environment*, 81, 166-176, 10.1016/j.atmosenv.2013.08.060, 2013.
- 25 Lefohn, A. S., Shadwick, D., and Oltmans, S. J.: Characterizing changes in surface ozone
26 levels in metropolitan and rural areas in the United States for 1980-2008 and 1994-2008,
27 *Atmospheric Environment*, 44, 5199-5210, 2010.
- 28 Li, J. F., Lu, K. D., Lv, W., Li, J., Zhong, L. J., Ou, Y. B., Chen, D. H., Huang, X., and
29 Zhang, Y. H.: Fast increasing of surface ozone concentrations in Pearl River Delta
30 characterized by a regional air quality monitoring network during 2006-2011, *Journal of*
31 *Environmental Science -China*, 26, 23-36, 2014.



- 1 Lin, M. Y., Horowitz, L. W., Payton, R., Fiore, A. M., and Tonnesen, G.: US surface ozone
2 trends and extremes from 1980 to 2014: quantifying the roles of rising Asian emissions,
3 domestic controls, wildfires, and climate, *Atmospheric Chemistry and Physics*, 17, 2943-
4 2970, 10.5194/acp-17-2943-2017, 2017.
- 5 Ling, Z. H., Guo, H., Lam, S., Saunders, S., and Wang, T.: Atmospheric photochemical
6 reactivity and ozone production at two sites in Hong Kong: Application of a Master Chemical
7 Mechanism–photochemical box model, *Journal of Geophysical Research - Atmospheres*, 119,
8 10567-10582, 2014.
- 9 Ling, Z. H., Guo, H., Zheng, J. Y., Louie, P. K. K., Cheng, H. R., Jiang, F., Cheung, K.,
10 Wong, L. C., and Feng, X. Q.: Establishing a conceptual model for photochemical ozone
11 pollution in subtropical Hong Kong, *Atmospheric Environment*, 76, 208-220,
12 10.1016/j.atmosenv.2012.09.051, 2013.
- 13 Liu, H., and Chan, J. C. L.: An investigation of air-pollutant patterns under sea–land breezes
14 during a severe air-pollution episode in Hong Kong, *Atmospheric Environment* 36, 591–601,
15 2002.
- 16 Liu, K.-Y., Wang, Z., and Hsiao, L.-F.: A modeling of the sea breeze and its impacts on
17 ozone distribution in northern Taiwan, *Environmental Modelling & Software*, 17, 21-27,
18 2002.
- 19 Lo, J. C. F., Lau, A. K. H., Fung, J. C. H., and Chen, F.: Investigation of enhanced cross-city
20 transport and trapping of air pollutants by coastal and urban land-sea breeze circulations,
21 *Journal of Geophysical Research-Atmospheres*, 111, 2006.
- 22 Lu, K. D., Zhang, Y. H., Su, H., Shao, M., Zeng, L. M., Zhong, L. J., Xiang, Y. R., Chang, C.
23 C., Chou, C. K. C., and Wahner, A.: Regional ozone pollution and key controlling factors of
24 photochemical ozone production in Pearl River Delta during summer time, *Science China*
25 *Chemistry*, 53, 651-663, 10.1007/s11426-010-0055-6, 2010.
- 26 Lu, X., Chow, K.-C., Yao, T., Lau, A. K. H., and Fung, J. C. H.: Effects of urbanization on
27 the land sea breeze circulation over the Pearl River Delta region in winter, *International*
28 *Journal of Climatology*, n/a-n/a, 10.1002/joc.1947, 2009a.
- 29 Lu, X., Chow, K. C., Yao, T., Fung, J. C. H., and Lau, A. K. H.: Seasonal variation of the
30 land-sea breeze circulation in the Pearl River Delta region, *Journal of Geophysical Research-*
31 *Atmospheres*, 114, 2009b.



- 1 Monks, P. S., Archibald, A. T., Colette, A., Cooper, O., Coyle, M., Derwent, R., Fowler, D.,
2 Granier, C., Law, K. S., Mills, G. E., Stevenson, D. S., Tarasova, O., Thouret, V., Von
3 Schneidemesser, E., Sommariva, R., Wild, O., and Williams, M. L.: Tropospheric ozone and
4 its precursors from the urban to the global scale from air quality to short-lived climate forcer,
5 Atmospheric Chemistry and Physics, 15, 8889-8973, 10.5194/acp-15-8889-2015, 2015.
- 6 NARSTO: An Assessment of Tropospheric Ozone Pollution-A North American Perspective,
7 NARSTO Management Office (Envair), Pasco, Washington, 2000.
- 8 NRC: Rethinking the Ozone Problem in Urban and Regional Air Pollution, National
9 Research Council, 1991.
- 10 Parrish, D. D., Trainer, M., Holloway, J. S., Yee, J. E., Warshawsky, M. S., Fehsenfeld, F. C.,
11 Forbes, G. L., and Moody, J. L.: Relationships between ozone and carbon monoxide at
12 surface sites in the North Atlantic region, Journal of Geophysical Research-Atmospheres, 103,
13 13357-13376, 1998.
- 14 Parrish, D. D., Law, K. S., Staehelin, J., Derwent, R., Cooper, O. R., Tanimoto, H., Volz-
15 Thomas, A., Gilge, S., Scheel, H. E., Steinbacher, M., and Chan, E.: Long-term changes in
16 lower tropospheric baseline ozone concentrations at northern mid-latitudes, Atmospheric
17 Chemistry and Physics, 12, 11485-11504, 2012.
- 18 Saunders, S. M., Jenkin, M. E., Derwent, R. G., and Pilling, M. J.: Protocol for the
19 development of the Master Chemical Mechanism, MCM v3 (Part A): tropospheric
20 degradation of non-aromatic volatile organic compounds, Atmospheric Chemistry and
21 Physics, 3, 161-180, 2003.
- 22 Seinfeld, J. H., and Pandis, S. N.: Atmospheric chemistry and physics: from air pollution to
23 climate change, John Wiley & Sons, 2016.
- 24 Shindell, D., Kuylenstierna, J. C. I., Vignati, E., van Dingenen, R., Amann, M., Klimont, Z.,
25 Anenberg, S. C., Muller, N., Janssens-Maenhout, G., Raes, F., Schwartz, J., Faluvegi, G.,
26 Pozzoli, L., Kupiainen, K., Hoglund-Isaksson, L., Emberson, L., Streets, D., Ramanathan, V.,
27 Hicks, K., Oanh, N. T. K., Milly, G., Williams, M., Demkine, V., and Fowler, D.:
28 Simultaneously Mitigating Near-Term Climate Change and Improving Human Health and
29 Food Security, Science, 335, 183-189, 10.1126/science.1210026, 2012.
- 30 Simpson, I. J., Blake, N. J., Barletta, B., Diskin, G. S., Fuelberg, H. E., Gorham, K., Huey, L.
31 G., Meinardi, S., Rowland, F. S., Vay, S. A., Weinheimer, A. J., Yang, M., and Blake, D. R.:



- 1 Characterization of trace gases measured over Alberta oil sands mining operations: 76
2 speciated C-2-C-10 volatile organic compounds (VOCs), CO₂, CH₄, CO, NO, NO₂, NO_y, O₃
3 and SO₂, *Atmospheric Chemistry and Physics*, 10, 11931-11954, 2010.
- 4 Skamarock, W. C., Klemp, J. B., Dudhia, J., Gill, D. O., Barker, D. M., Duda, M. G, Huang,
5 X.-Y., Wang, W., and Powers, J. G.: A Description of the Advanced Research WRF Version
6 3. NCAR Tech. Note NCAR/TN-475+STR, 113 pp. doi:10.5065/D68S4MVH, 2008.
- 7 Stein, A.F., Draxler, R.R, Rolph, G.D., Stunder, B.J.B., Cohen, M.D., and Ngan, F.: NOAA's
8 HYSPLIT atmospheric transport and dispersion modeling system, *Bulletin of American*
9 *Meteorological Society*, 96, 2059-2077, 2015.
- 10 Velchev, K., Cavalli, F., Hjorth, J., Marmer, E., Vignati, E., Dentener, F., and Raes, F.:
11 Ozone over the Western Mediterranean Sea – results from two years of shipborne
12 measurements, *Atmospheric Chemistry and Physics*, 11, 675-688, 10.5194/acp-11-675-2011,
13 2011.
- 14 Wang, N., Guo, H., Jiang, F., Ling, Z. H., and Wang, T.: Simulation of ozone formation at
15 different elevations in mountainous area of Hong Kong using WRF-CMAQ model, *Science*
16 *of the Total Environment*, 505, 939-951, 2015.
- 17 Wang, T., LAM, K. S., and LEE, A. S. Y.: Meteorological and Chemical Characteristics of
18 the Photochemical Ozone Episodes Observed at Cape D'Aguilar in Hong Kong, *Journal of*
19 *Applied Meteorology*, 30, 1167-1178, 1998.
- 20 Wang, T., Guo, H., Blake, D. R., Kwok, Y. H., Simpson, I. J., and Li, Y. S.: Measurements of
21 Trace Gases in the Inflow of South China Sea Background Air and Outflow of Regional
22 Pollution at Tai O, Southern China, *Journal of Atmospheric Chemistry*, 52, 295-317,
23 10.1007/s10874-005-2219-x, 2005.
- 24 Wang, T., Wei, X. L., Ding, A. J., Poon, C. N., Lam, K. S., Li, Y. S., Chan, L. Y., and Anson,
25 M.: Increasing surface ozone concentrations in the background atmosphere of Southern China,
26 1994-2007, *Atmospheric Chemistry and Physics*, 9, 6217-6227, 2009.
- 27 Wang, Y., Guo, H., Zou, S., Lyu, X., Wang, H., Ling, Z., and Cheng, H.: Ground level O₃
28 photochemistry over South China Sea: Application of a near-explicit chemical mechanism
29 box model, *Environmental Pollution*, under revision, 2017b.



- 1 Wang, Y., Wang, H., Guo, H., Lyu, X., Cheng, H., Ling, Z., Louie, P. K. K., Simpson, I. J.,
2 Meinardi, S., and Blake, D. R.: Long term O₃-precursor relationships in Hong Kong: Field
3 observation and model simulation, *Atmospheric Chemistry and Physics*, 17(18), 10919-
4 10935, 2017a.
- 5 Wei, X., Lam, K.-S., Cao, C., Li, H., and He, J.: Dynamics of the Typhoon Haitang Related
6 High Ozone Episode over Hong Kong, *Advances in Meteorology*, 2016, 1-12,
7 10.1155/2016/6089154, 2016.
- 8 WHO: Health aspects of air pollution with particulate matter, ozone and nitrogen dioxide:
9 report on a WHO working group, Bonn, Germany 13-15 January 2003, World Health
10 Organization, 2003.
- 11 Willmott, C. J.: Some comments on the evaluation of model performance, *Bulletin of the*
12 *American Meteorological Society*, 63(11), 1309-1313, 1982.
- 13 Xu, X., Lin, W., Wang, T., Yan, P., Tang, J., Meng, Z., and Wang, Y.: Long-term trend of
14 surface ozone at a regional background station in eastern China 1991-2006: enhanced
15 variability, *Atmospheric Chemistry and Physics*, 8, 2595-2607, 2008.
- 16 Yang, J. X., Lau, A. K. H., Fung, J. C. H., Zhou, W., and Wenig, M.: An air pollution episode
17 and its formation mechanism during the tropical cyclone Nuri's landfall in a coastal city of
18 south China, *Atmospheric Environment*, 54, 746-753, 10.1016/j.atmosenv.2011.12.023, 2012.
- 19 Yin, L. H.: Analysis of Meteorological Criteria Leading to Tropical Cyclone Related Ozone
20 Episodes in Hong Kong, PhD, HKUST, 2004.
- 21 Zhang, M., and Zhang, L.: Study of the sea-land breeze system in Hong Kong, *Hong Kong*
22 *Meteorological Society Bulletin*, 22-42, 1997.
- 23 Zhang, Q., Yuan, B., Shao, M., Wang, X., Lu, S., Lu, K., Wang, M., Chen, L., Chang, C. C.,
24 and Liu, S. C.: Variations of ground-level O₃ and its precursors in Beijing in summertime
25 between 2005 and 2011, *Atmospheric Chemistry and Physics*, 14, 6089-6101, 10.5194/acp-
26 14-6089-2014, 2014.
- 27 Zheng, J. Y., Zhong, L. J., Wang, T., Louie, P. K. K., and Li, Z. C.: Ground-level ozone in
28 the Pearl River Delta region: Analysis of data from a recently established regional air quality
29 monitoring network, *Atmospheric Environment*, 44, 814-823, 2010.

30